frontiers | Frontiers in Earth Science

TYPE Original Research
PUBLISHED 14 September 2023
DOI 10.3389/feart.2023.1239689

OPEN ACCESS

EDITED BY
Hu Wang,
Southwest Jiaotong University, China

REVIEWED BY
Yikang Zheng,
Institute of Geology and Geophysics (CAS), China
Xuzhang Shen,
Sun Yat-sen University, China
Mikhail Rodkin,
Institute of Earthquake Prediction Theory and Mathematical Geophysics (RAS), Russia

*CORRESPONDENCE
Zhujun Han,
zjhan0904@163.com

†PRESENT ADDRESS
Zhangdi Xie,
College of Earth and Planetary Sciences, University of Chinese Academy of Sciences, Beijing, China

RECEIVED 13 June 2023
ACCEPTED 21 August 2023
PUBLISHED 14 September 2023

CITATION
Dong S, Han Z, Guo P, Xie Z and Yin X (2023), Seismological research in Yunnan Province, China, and its tectonic implication between the Xianshuihe-Xiaojiang fault system and the Red River fault zone.
Front. Earth Sci. 11:1239689.
doi: 10.3389/feart.2023.1239689

Seismological research in Yunnan Province, China, and its tectonic implication between the Xianshuihe-Xiaojiang fault system and the Red River fault zone

Shaopeng Dong[1,2], Zhujun Han[1,2]*, Peng Guo[1,2], Zhangdi Xie[1,2†] and Xinzhong Yin[1,3]

[1]Institute of Geology, China Earthquake Administration, Beijing, China, [2]Key Laboratory of Seismic and Volcanic Hazards, China Earthquake Administration, Beijing, China, [3]State Key Laboratory of Earthquake Dynamics, Institute of Geology, China Earthquake Administration, Beijing, China

The tectonic crosscutting relationship between the two most tectonic important Xianshuihe-Xiaojiang fault system (XFS) and the Red River fault zone (RRF) is a key basic problem but it is controversial now. These obscure further leads to a hot argument about the geodynamic model of the southeast margin of the Tibetan Plateau. In order to answer whether the XFS has cut across the RRF and extended southwardly, multiple seismological methods, including seismic relocation, b-value analysis, seismic energy, density study, focal mechanism inversion, and regional stress field research, are applied in the Yunnan Province area, China, where the XFS and the RRF intersects with each other. The results comprehensively demonstrate that the southern segment of the XFS has not been affected by the RRF, and it has continued for a length after crossing the RRF, but the Dian Bien Phu fault zone should not be an extension fault of the XFS. Along the SW direction, starting from the middle segment of the XFS, and cutting across the Qujiang fault, Shiping-Jianshui fault zone, RRF, Ailaoshan fault zone, Wuliangshan fault zone, and the southern section of the Daluo fault, the belt should be treated as the eastern boundary of the clockwise rotational in geodynamics model of the Tibetan Plateau in this study area. Based on these conclusion above and previous recognitions, a new geodynamic evolution model is proposed.

KEYWORDS

Xianshuihe-Xiaojiang fault system, Red River fault zone, geodynamic model, seismological analysis, Yunnan Province and its adjacent area

1 Introduction

The southeast margin of the Tibetan Plateau, characterized by complex Cenozoic structures created during the Indo-Asia collision (Molnar and Tapponnier, 1975; Yin and Harrison, 2000; Schoenbohm et al., 2006), is particularly important for understanding the tectonic evolution and uplift of the plateau (Wang et al., 1998). Various geodynamic models (Molnar and Tapponnier, 1975; Peltzer and Tapponnier, 1988; Royden et al., 1997; Flesch et al., 2001; Replumaz and Tapponnier, 2003; Copley, 2008; Wen et al., 2011; Shi et al., 2018b) have been proposed to describe the nature of continental deformation probably due to the unclear recognition on this area. What is

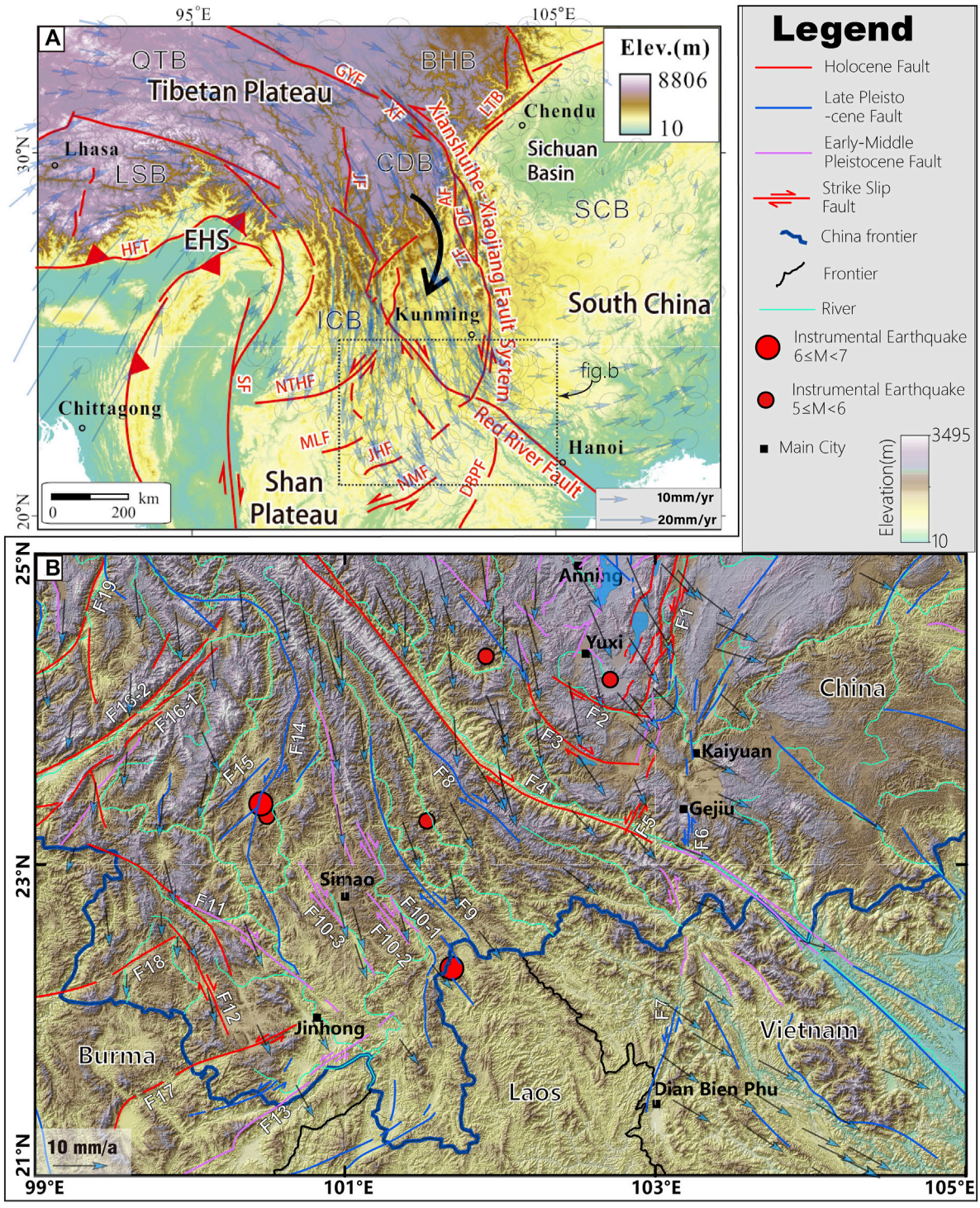

FIGURE 1
The sketch geologic map of the southeast Tibetan Plateau area **(A)** and study region **(B)**. The fault distribution is modified from the Seismic ground motion parameter zonation map of China. (2015). The earthquake data are cited from the China Earthquake Networks Center. The GPS data applied in Figures A and B were cited from Gan et al. (2021). The GPS velocity field is relative to a "Tibetan Plateau-fixed" reference frame, which highlights the E-W extension across the plateau and clockwise rotation in its eastern part. Abbreviations: BHB=Bayan Har Block, CDB=Chuandian Block, QTB=Tiangtang Block, LSB=Lhasa Block, SCB=South China Block, ICB=Indochina Block, AF=Anninghe Fault, DBPF= Dian Bien Phu Fault, DF=Daliangshan Fault, GYF=Ganzi-Yushu Fault, HFT=Himalayas Frontal Thrust, JF=Jingshajiang fault, JHF=Jinghong Fault, LTB=Longmengshan Thrust Belt, MLF=Menglian Fault, NMF=Mae Chan Fault, NTHF=Nangtinghe Fault, SF=Sagaing Fault, XF=Xianshuihe Fault, XF=Xiaojiang Fault, ZF=Zemuhe Fault, EHS=Eastern Himalayan Syntaxis, F1=Middle segment of the XFS, F2=Qujiang Fault; F3=Shiping-Jianshui Fault; F4=RRF; F5=South segment of the XFS, F6=Gejiu Fault, F7=Dian Bien Phu Fault; F8=Ailaoshan Fault; F9=Babianjiang Fault, F10=Wuliangshan Fault, F10-1=Mohei Fault (East branch), F10-2=Puer Fault (Middle branch), F10-3=Puwen Fault (West branch), F11=Heihe Fault, F12=Longling-Lancang Fault, F13=Menglong Fault, F14=Lancangjiang Fault, F15=Jinggu Fault, F16=Nantinghe Fault, (F16-1=East branch, F16-2=West branch), F17=Daluo Fault, F18=Menglian Fault, and F19=Wandin Fault.

accepted by almost all geologists is that GPS results demonstrated significant clockwise rotation in the margin between the eastern Himalayan syntaxis (EHS) and the left-lateral strike-slip Xianshuihe-Xiaojiang Fault System (Shen et al., 2005; Wang et al., 2008; Gan et al., 2021), revealing the present clockwise rotation of the upper crust of the southeast margin of the Tibetan Plateau around the EHS (Zhang et al., 2004).

In the southeast margin of the Tibetan Plateau region, the two most important and significant tectonic systems are the Red River Fault (RRF) and Xianshuihe-Xiaojiang Fault System (XFS), composed of Xianshuihe Fault in the north, Daliangshan Fault, Anninghe Fault, and Zemuhe Fault in the middle, and Xiaojiang Fault system (XFS) in the south (Figure 1). In the past decades, aiming at the crosscutting relationship between the RRF and XFS in the present tectonic movement, which is also the key base problem here, many researchers have proposed various heuristic geodynamic models as mentioned above. All these models can be generalized into two types. One type supports the almost N-S striking XFS that has not cut across the NW striking RRF, and the left lateral movement of the XFS ended at the south segment of the XFS and north of the RRF, meaning the RRF is predominant in the present tectonic deformation in the southeast margin of the Tibetan Plateau (Li and Wang, 1975; Tapponnier et al., 1982; He et al., 1992; Li, 1993; Roger et al., 1995; Song and Wang, 1998; Replumaz et al., 2001; Xu et al., 2003; Zhang et al., 2003; Wen et al., 2011; Xu et al., 2011). The other type suggests that the left lateral movement of the XFS has cut across the RRF and connected with a series of NE striking faults at the southwest of the RRF, forming the predominant left lateral tectonic belt (Lacassin et al., 1998; Wang et al., 1998; Chen et al., 2000; Schoenbohm et al., 2004; Shen et al., 2005; Schoenbohm et al., 2006; Simons et al., 2007; Wu et al., 2015; Zhang and Ding, 2016). So, the crosscutting relationship between the RRF and the XFS is the key base to the present geodynamic models, which is also the aim of this study.

Recently, our group obtained paleoseismic evidence (Guo et al., 2021b), geologic slip rate (Han et al., 2017), and tectonic geomorphologic characteristics (Guo et al., 2021a) of Holocene faulting activity of the Jianshui Fault, south segment of the Xiaojiang Fault, suggesting the strong faulting activity of the Jianshui Fault. Here, the present crosscutting relationship between the RRF and XFS is discussed from a seismological scope.

2 Data and methods

A total of 24,543 raw earthquakes (ML≥0.5) in the period from 1 January 2009, to 31 October 2017, were selected from the seismic phase report of Yunnan Province in the study region (21°N~25°N, 99°E~105°E). After testing the completeness of the earthquake catalog (Rydelek and Sacks, 1989), the smallest magnitude interval Mc was determined at Mc 1.3 (Figure 2D), below which the magnitude-cumulative frequency relationship does not obey Gutenberg-Richter law (Gutenberg and Richter, 1944). After filtering, a total of 15,208 earthquakes M≥1.3 were chosen (Figure 2). In order to identify the tectonic relationship between the XFS and RRF, several regular seismic methods, including seismic relocation, spatial distribution of b value, seismic energy, density distribution analysis, focal mechanism solution analysis, regional stress field inversion, were comprehensively obtained to further analyze the seismic characteristics along the XFS and the RRF. Detailed technical information, including parameters used, detailed meaning, and description of the treating processes can be found in supporting documents.

3 Results and preliminary analysis

3.1 Crust velocity model and relocation results

As described above, three crust velocity models have been applied in our research, which are PREM (Dziewonski and Anderson, 1981), AK135 (Kennett et al., 1995), and the modified regional model (Hu and Han, 2013). The wave velocity ratio (Vp/Vs) of the PREM and AK135 model is set as 1.75, while it is 1.96 in the HN model. Because the picking accuracy of P-wave travel time data is better than S-wave, the weighting value of P-wave in relocation is set at 1, while it is set at 0.7 for S-wave. Considering a large number of earthquake events from the catalog, the LSQR algorithm (Paige and Saunders, 1982), belonging to the family of conjugate gradient methods, was used to solve the equation. This method has also been applied successfully in a previous study (Yao et al., 1999). Considering the possible comparatively large error of the initial relocation result, eight times iteration in two groups was applied in the solution. Because the relocation needs to pair earthquakes within a certain distance in the study region, different relocation parameters lead to different relocation results. The null relocation results are mainly caused by overlarge distance with other earthquakes in the iterative inversion process (Waldhauser and Ellsworth, 2000).

After the pretreatment and program calculation, a total of 491,691 pairs of P-wave and 408,278 S-wave seismic phases were obtained from 619,562 pairs of original P-wave and 587,468 S-wave seismic phases, meaning the matching rates are 79% and 69%, respectively, and the average distance between event pair is 4.87 km.

The minimum seismic phase pair number that forms a swarm was set as four in 15,208 events involved in relocation, and 1,009 events, considered isolated events, were removed from relocation due to dissatisfaction with the minimum number. Some events were also removed in 14,199 events after filtering. The detailed parameters used in relocation and their process are illustrated in the supporting document. Finally, 11,531, 11,535, and 12,080 events were obtained after relocation based on PREM, AK135, and HN crust velocity models, respectively. The spatial distribution map of these events from these three velocity models is shown in Figure 3. Compared with the spatial distribution map of the events before the relocation (Figure 3A), we could see that the horizontal distribution of events before the relocation was more discrete, and the difference between the spatial distribution map of events based on three crust velocity models was not that obvious (Figures 3B–D), revealing the result stability of this relocation.

After relocation, regnant depth based on three velocity models was more concentrated. Considering the event number and average residue after relocation based on the same raw earthquake events, the PREM velocity model is better (Table 1). According to research on the parameters in double difference hypocenter relocation, Zheng

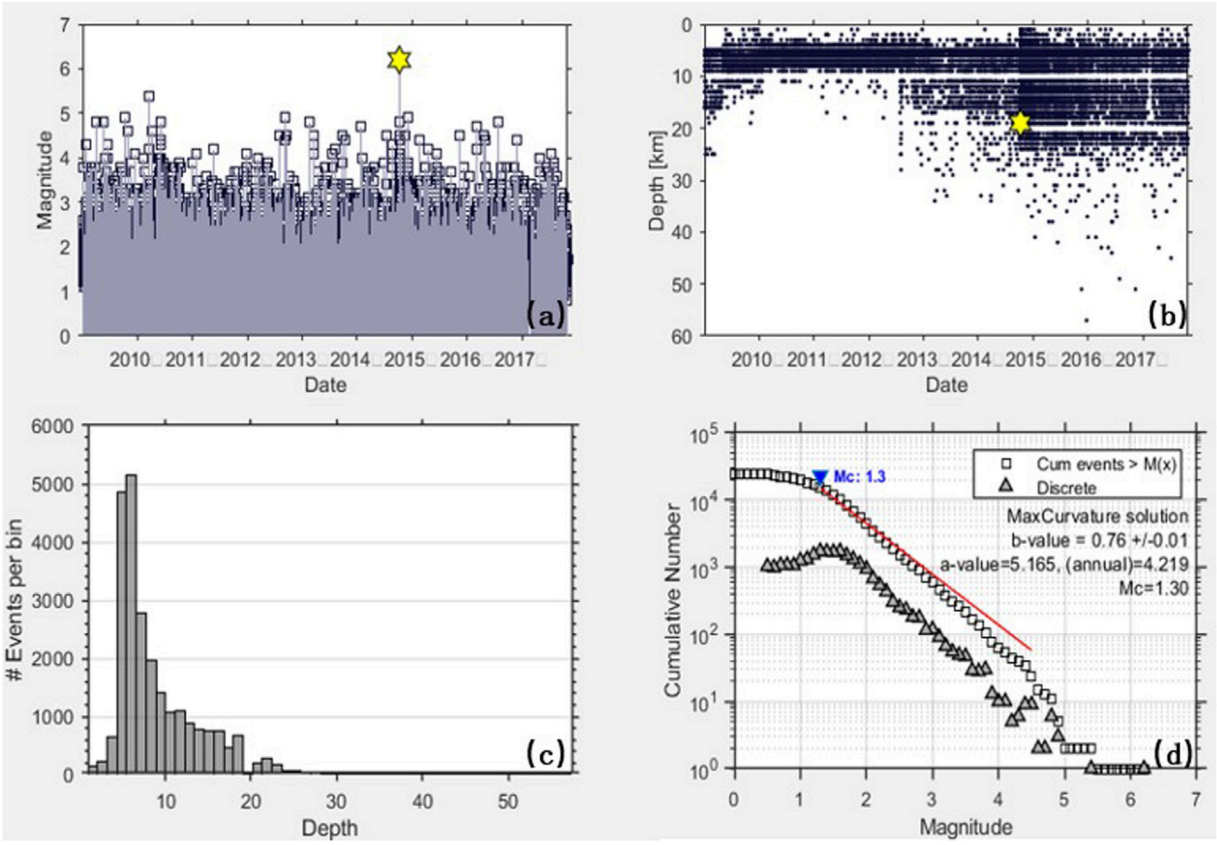

FIGURE 2
The statistical characteristic charts of the raw earthquake catalog data, date-magnitude chart **(A)**, date-epicenter depth chart **(B)**, epicenter depth-earthquake number chart **(C)**, and magnitude-frequency chart **(D)**. The yellow star is the biggest instrumental earthquake in the study region, October 2014 M6.6 Jinggu Earthquake.

and Yang (2008) concluded that double difference hypocenter relocation matched better with the PREM velocity model, in which a low-velocity layer existed on the surface of the earth. After comparison among the three velocity models above, the result from the PREM model had more events and smaller errors after relocation. We accepted the PREM model and used the resulting relocation data in the following study.

3.2 B-value result

The b-value distribution map was obtained through the fixed Mc (1.3) method. After the relocation, b-value increased at the same locations, probably because the relocation made the events more concentrated (Figure 4). The b-value distribution map after relocation (Figure 4B) showed high b-value characteristics from the middle segment of the Red River Fault to the south segment of Xiaojiang Fault and Gejiu Fault, meaning there is a comparatively low possibility of strong earthquake occurrence generally in this region. Low b-value existed along the Qujiang Fault, meaning a comparatively higher possibility of strong earthquake occurrence.

3.3 Seismic energy and density result

From the seismic energy distribution maps (left charts in Figure 5) and the events density distribution maps (right charts in Figure 5), an anomalous belt exists (the area between two black lines in Figure 5). The spatial characteristics of seismic energy and density distribution maps could recently reveal the relationship between seismic activity characteristic and faults trace and the possible trend of seismic activity in the future.

From Figure 5, we can tell that 1) the seismic activity along the middle segment of the RRF, the area between the middle segment of the XFS and Gejiu Fault, is mainly consistent with the fault trace; 2) an NE-striking anomalous seismic activity belt exists along the middle segment of the XFS, extending across Qujiang Fault, Shiping-Jianshui Fault, RRF, Ailaoshan Fault, Babianjiang Fault, and Puwen Fault to the south side of Lancang-Gengma Fault.

The main epicenter locations and depth information could be obtained from seismic profiles, usually from which underground geological structures and rupture traces could be depicted. In order to know whether the earthquake belt along the Xiaojiang Fault system had extended across the Red River Fault, three seismic profiles were set across the Xiaojiang Fault system and its

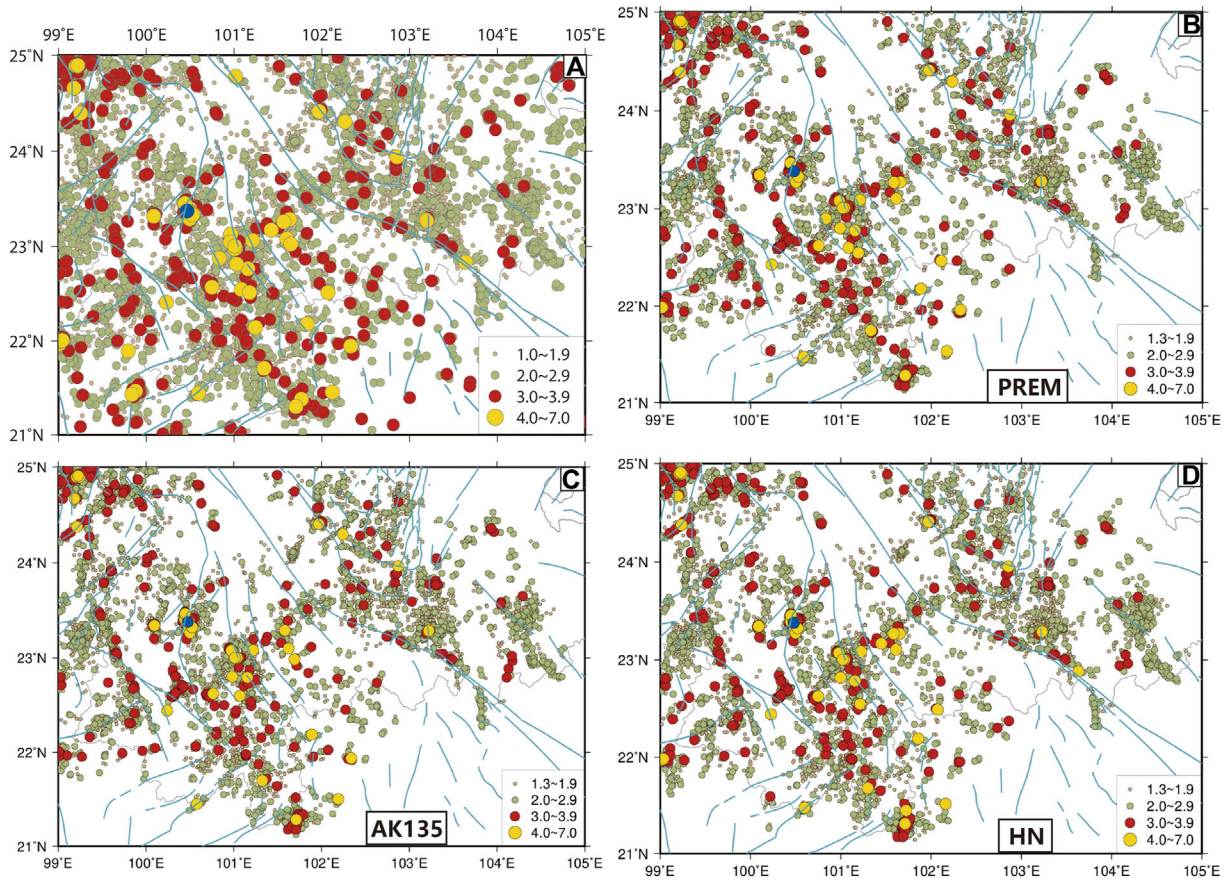

FIGURE 3
Seismic events distribution map before **(A)** and after relocation with different crust velocity models, PREM velocity model **(B)**, AK135 velocity model **(C)**, and regional velocity model **(D)**.

TABLE 1 The statistical result of the relocation result and error with three different velocity models.

Velocity models	Events obtained	Error at three component directions/km		
		E-W	N-S	Z
PREM	11,531	0.095	0.092	0.095
AK135	11,535	0.142	0.141	0.133
HN	12,080	0.317	0.314	0.394

elongation (Figure 6), and statistical analysis was made in the regions that defined 10km and 20 km on both lateral sides to detect the underground structure.

Based on earthquake energy and density distribution map results, three earthquake density distributions along the profiles are obtained (Figures 7–9). From the profiles, we find that 1) the epicenter depth is consistent from NE to SW, mainly concentrating at 0–15 km; 2) a high earthquake density belt, probably meaning a geologic structure, exists on all three profiles; 3) the depth of the high earthquake density belt increases and then decreases from NE to SW.

3.4 Focal mechanism solution result and analysis

Based on the relocation result from the HN velocity model, a total of 5,532 events (1.3≤M≤6.2) were used in focal mechanism solution inversion. The waveform between 10s before and 50s after every event was used in inversion, and parameters used in strong earthquake inversion were applied, and a total of 5,466 focal mechanism solutions were obtained (Figure 10). All focal mechanism solutions were classified according to classification standard (Zoback, 1992) (Table 2).

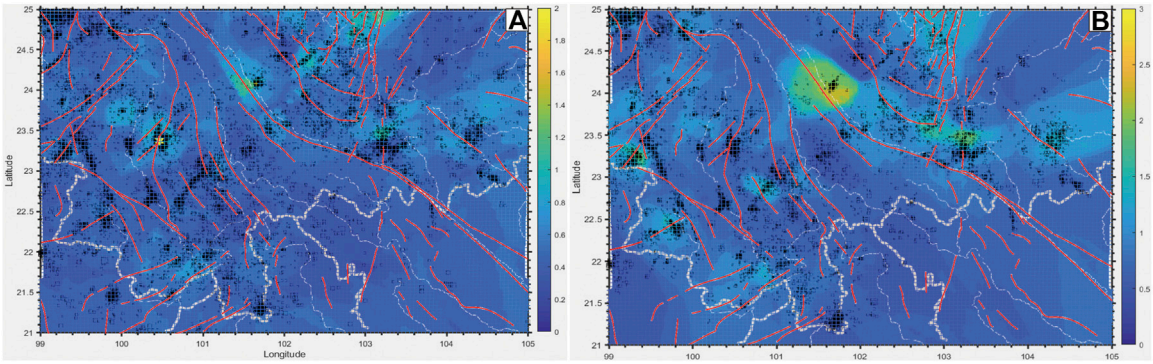

FIGURE 4
The b-value distribution map before **(A)** and after **(B)** relocation.

Because crust structure and stress field may differ in different areas, one set of statistical results from the whole region is probably not enough to extract the tectonic information needed, and the magnitude of focal mechanism solutions is small, which cannot be used to compare with data published from other seismic organizations. Here, ensuring the same parameters in inversion, we compared our result with previous research (Hu and Han, 2013), the study region of which is located in our study region, to check the reliability of our result.

Hu and Han (2013) obtained 148 focal mechanism solutions inversion (ML≥2.0) of events in the arcuate tectonic belt in southeast Yunnan (23°N-25°N, 101°E-103°E; the black rectangle in Figure 11). Here, we picked out 230 focal mechanism solutions (ML≥2.0) from the same area to compare. The statistical analysis from both groups of data showed that the results from our research were very consistent with the result from Hu and Han (2013), revealing that normal faulting was dominant there and the tensile stress in the SWW-NEE direction plays a more important role in present-day activity of the arcuate tectonics compared to the compressive stress in the SSE-NNW direction.

Since the RRF is considered a very important tectonic boundary and its tectonic relationship with XFS is still in hot debate as described above, the tectonic belt along the Xiaojiang Fault zone and its elongation (the area between the two black lines in Figure 12) was divided into two subregions in order to check whether the Red River fault is still blocking the tectonic extension of the Xiaojiang Fault zone. The subregion north of the RRF is shown as black focal mechanism solutions while the south of the RRF is red (Figure 12).

Based on the fault nature classification principles from the base of hypocenter theory (Chen and Chen, 1999), the statistical characteristic of the focal mechanism solutions of two subregions (Figure 13) shows that the percentage of normal faulting of nodall in the subregion south of the RRF is 53%, and the percentage of nodal II is 52%; while the percentage of normal faulting of nodal I in the subregion north of the RRF is 52% and the percentage of nodal II is 51%. This means the normal faulting earthquake is predominant in the region. Almost the same statistical characteristic between the subregions besides the RRF revealed the consistent stress field characteristic.

Combining the earthquake energy, density distribution charts (Figures 11–13), and the statistical analysis on focal mechanism solutions above, we can deduce that the tectonic blocking from the RRF does not exist presently.

3.5 Stress field result

Based on previous researchers' experience (Hardebeck and Michael, 2004), the study region was divided into 1,026 mesh grids (grid size 0.15°*0.15°), and the optimal fitting tectonic stress tensor of every grid was calculated. According to the equation from Lund and Townend (2007), horizontal maximum principal compressive stress map was obtained. The focal mechanism solutions distribution of small events in the study region (Figure 14) shows that focal mechanism solutions are distributed in most study regions evenly. The main faulting type of the focal mechanism solutions in the distribution map distributes very dispersively, which is probably related to the small magnitude of the events used in this study. The small events that release small energy are easily affected by local factors, meaning local structure information is predominant.

From the R-value distribution map (Figure 15), the R-value distributes dispersively and is generally larger than 0.5, meaning the maximum principal compressive stress status is stable (Huang et al., 2016). R-value is high along middle and south segments of XFS and Gejiu fault, meaning there is strong tectonic activity presently, and the area where R-value maintains around 0.5 distributes along RRF, Qujiang Fault, Shiping-Jianshui Fault, Ailaoshan Fault, Babianjiang Fault, and the south segment of Lancang-Gengma Fault, which is consistent with the anomalous belt of seismic density and seismic energy above (Figure 5).

4 Discussion

4.1 The information from seismological statistics

According to the results of the relocation and focal mechanism solutions, some zonation and linear tectonic characteristics could be revealed:

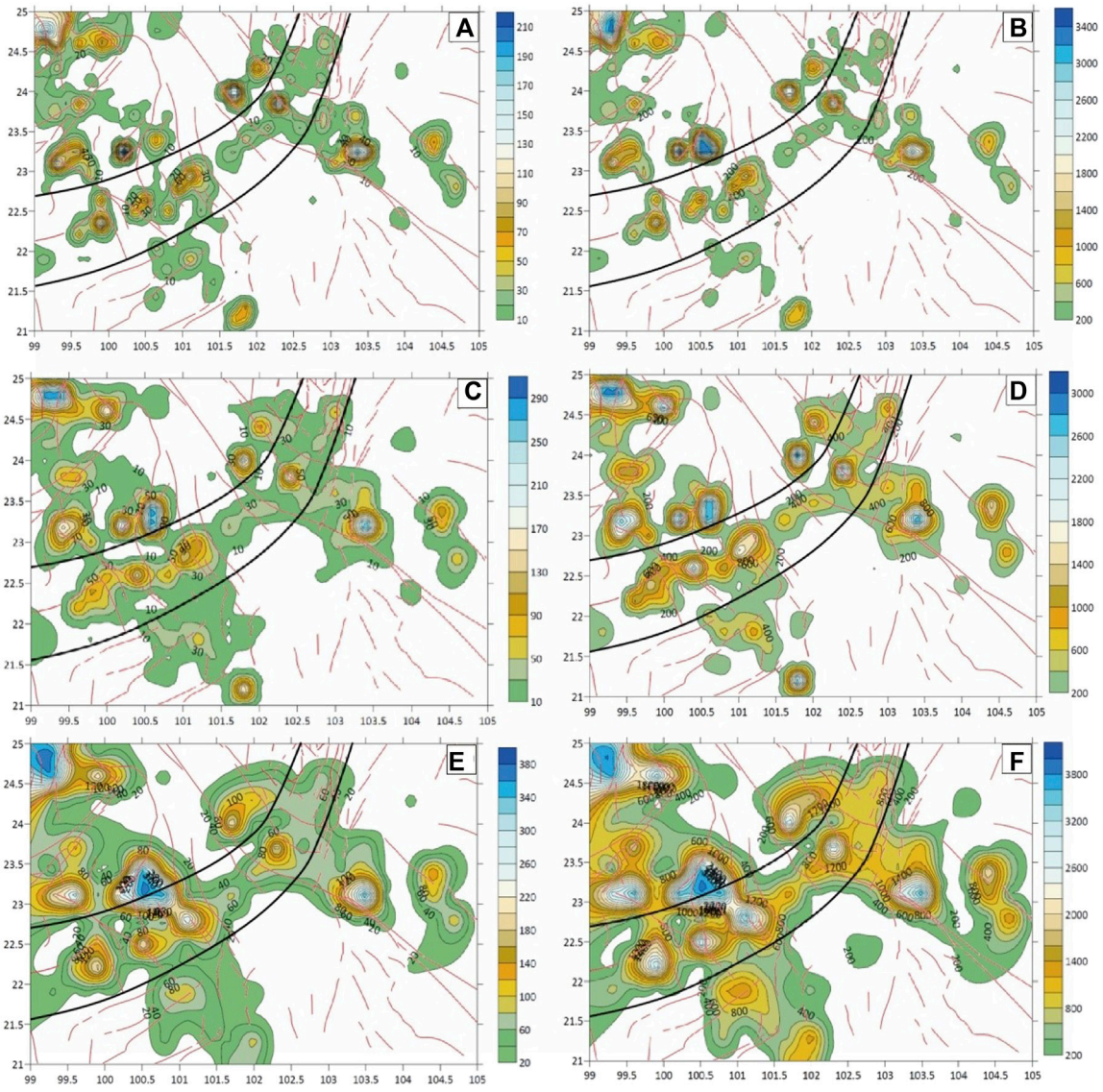

FIGURE 5
Seismic events density **(A,C,E)** and seismic energy **(B,D,F)** distribution maps of the study region. The first-row charts **(A,B)** are the results of 0.15°*0.15° mesh grids, the second-row charts **(C,D)** are 0.2°×0.2° mesh grids, while the third-row charts **(E,F)** are 0.3°×0.3° mesh grids.

1) In the area from the middle and south segments of XFS to Gejiu Fault and from east RRF to Qujiang Fault and Shiping-Jianshui Fault, small earthquake activity is strong, and the principal compressive stress field has the characteristics of mainly NE striking and local NW striking.
2) In the area of the Longling-Gengma fault and its west side, some strong earthquakes occurred there earlier (Shao et al., 2015), and in recent years, small earthquakes have been dense there, mainly along Lancang-Gengma (NW direction). The stress field in this region is predominantly NE direction and locally NW direction.
3) Seismic energy and density distribution characteristics in the area from the middle segment of the XFS to Longling-Gengma fault, across a series of NW striking fault, such as Qujiang fault, Shiping-Jianshui fault, RRF, Ailaoshan fault, Babianjiang fault, and Longling-Gengma fault, are very familiar, and the stress field direction changes from NW at XFS to NE at Longling-Gengma fault.

The relocation and seismic energy and density distribution maps revealed the seismic activity characteristic in recent years, and the profiles revealed geological structures underground. The stress field reflected from this study is also consistent with previous cognition of the stress field. The current research on tectonic stress field in the Chuandian region (Kan et al., 1977; Cheng, 1981; Xu et al., 1989; Xu, 1995; Cheng et al., 2003; Xie et al., 2004) revealed that the northward pushing of Indochina block, the southeastward left lateral movement of material in Tibetan Plateau, the blocking of South China Block, and the dragging of Burma Block jointly resulted in two stress transition belts at the eastern and western sides of the Chuandian Block. The principal compressive stress of the eastern

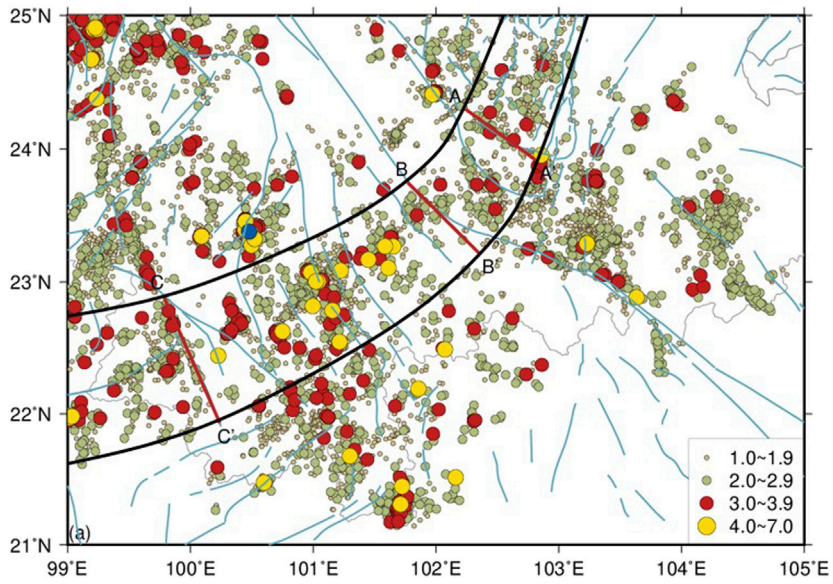

FIGURE 6
The seismic profile location on seismic energy and seismic density map. Profiles: AA', BB', and CC'.

and western sides of Chuandian Block obtained in this study is consistent with the background tectonic stress field, which suggested that the principal compressive stress is mainly NW trending at the eastern side of Chuandian Block while mainly NNE at the western side of Chuandian Block (Luo et al., 2014).

The following regional characteristics could be achieved as follows:

1) In the north of the RRF, the middle and south segments of the XFS are the boundary. The seismic energy and density distribution maps (Figure 9) show strong seismic activity and dense seismic energy at the middle and south segments of the XFS, where the large R-value from the focal mechanism (Figure 15) also exists, fitting with strong tectonic activity there. In the west of this boundary, the maximum compressive stress is mainly NW striking, while the east of this boundary is mainly NE striking, which is consistent with previous research. Strong small earthquake activity near the Qujiang Fault and Shiping-Jianshui Fault exists due to NW striking extrusion force from the north. At the perpendicular direction of NW principle compressional stress, shearing fracture and following tensional stress will occur according to the Hooke law, meaning tensional stress should be predominant there, which is consistent with a previous study and this research in this region (Hu and Han, 2013). This may be explained by the finding that the joint compressional stress from NW-striking principal stress in the east of the RRF and stronger NW-striking principal stress at the southeast side of the middle and south segments of the XFS resulted in enhanced inner vertical tensional stress with local characteristics of normal faulting in this region.
2) On the southwest side of the RRF, the Dian Bien Phu Fault is considered the boundary in previous geodynamic models, in which clockwise rotation around the EHS cut across the RRF and these models are strongly supported by GPS observations (Iwakuni et al., 2004; Shen et al., 2005; Simons et al., 2007; Zhang and Ding, 2016). The seismic energy and density distribution maps suggest that seismic activity does not extend along the Dian Bien Phu Fault after distributing along the south segment of the XFS and Gejiu Fault and across the RRF. However, the regional principal compressive stress direction in the area of the south segment of the XFS, Gejiu Fault, and Dian Bien Phu Fault is all NW-striking, which is consistent with previous research (Guo et al., 2014; Luo et al., 2014). The focal mechanism inversed from seismic data after relocation shows almost the same stress field direction besides the Dian Bien Phu Fault, meaning the region beside the Dian Bien Phu Fault is generally suffering NW-striking principal compressive stress and the fault is playing a whole role in the clockwise rotation system of the southeast margin of Tibetan Plateau.
3) At the area beside the RRF, or Qujiang Fault, Shiping-Jianshui Fault, Ailaoshan Fault, and Wuliangshan Fault, the seismic energy and density distribution maps show very good continuity. The R-value is mainly bigger than 0.5 in this region while smaller beside this region, meaning small earthquake activity in this region is strong. When considering the boundary from the middle and south segments of the XFS at the northeast side of the RRF and south end of Wuliangshan Fault to Menglong Fault, the NE striking belt across Qujiang Fault, Shiping-Jianshui Fault, RRF, Ailaoshan Fault, Babianjiang Fault, Wuliangshan Fault, and Longling-Gengma Fault could be treated as a whole region with consistent seismic energy, density, and R-value distribution. The principal compressive stress direction gradually changes from NW at the Qujiang Fault to NE at the south part of the Longling-Gengma Fault. Seismic density profiles demonstrate that a continuous deep tectonic belt exists inside, and earthquakes beside this belt occur in the shallow crust while the depth of the seismic events in the belt is comparatively deeper.

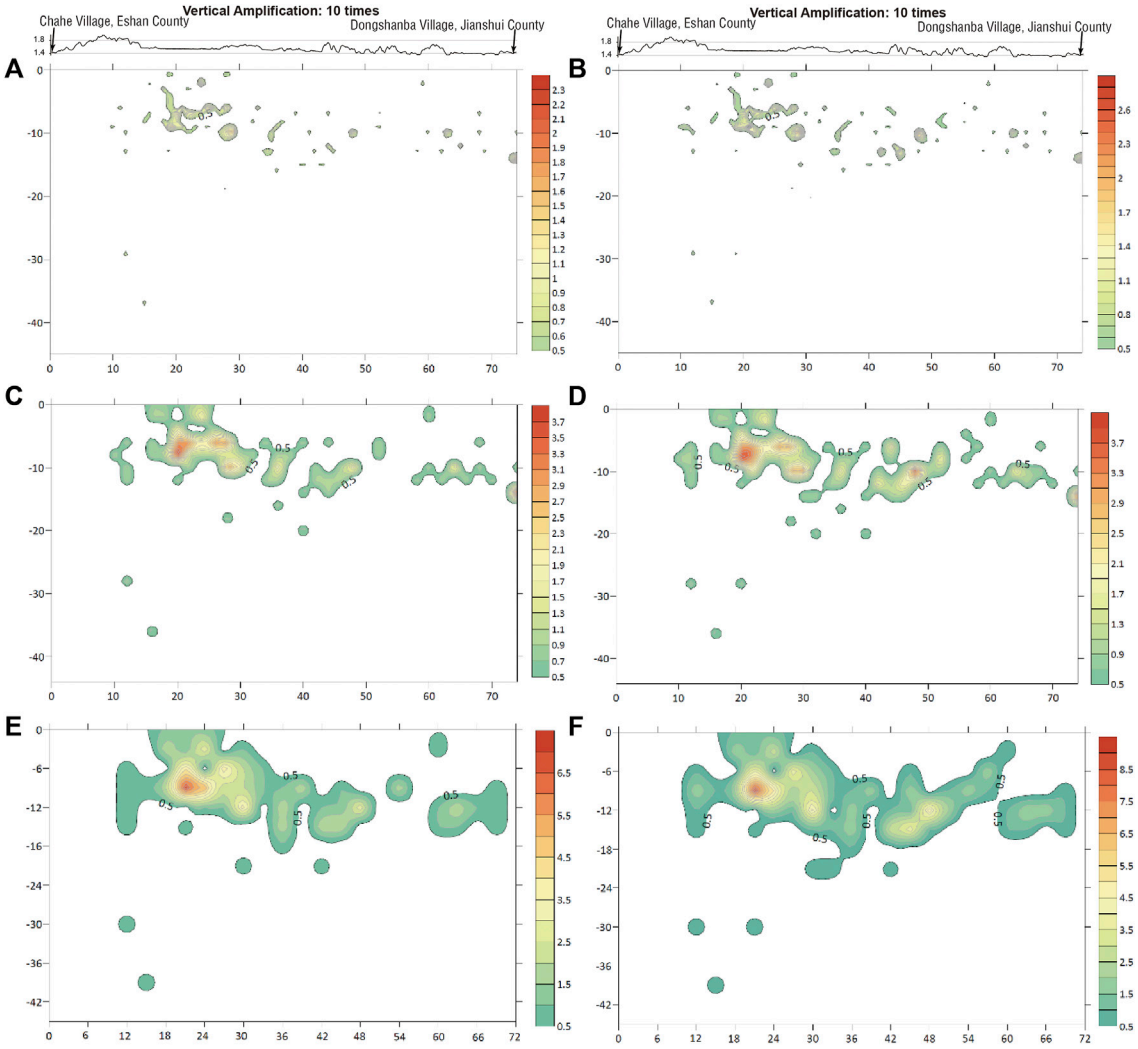

FIGURE 7
Earthquake energy isolines map along profile A-A′. The upper charts are the geomorphological profile along A-A′ and its settlement sites. The left charts **(A,C,E)** are the results in the region on 10 km lateral sides of A-A′ while the right charts **(B,D,F)** are the results on 20 km. The mesh grid size of charts a and b is 1 km*1km, charts c and d is 2 km*2km, and charts e and f is 3 km*3 km. The unit of both axes is km.

4.2 The implication of the geodynamic model of the southeast margin of the Tibetan Plateau

This study involves the two most important and significant fault systems, RRF and XFS, which are composed of the Xianshuihe Fault in the north and the Xiaojiang Fault in the south. Current research reveals different tectonic activities of these two fault systems nowadays. Abundant GPS observations have clearly demonstrated the strong systematic sinistral movement of the XFS (Zhang et al., 2004; Shen et al., 2005; Simons et al., 2007; Wang et al., 2008; Gan et al., 2021), and strong Holocene faulting activity of the XFS (He and Ren, 2003; Shen et al., 2003; He et al., 2006; He and Ikeda, 2007; He et al., 2008; He and Oguchi, 2008; Ren et al., 2010; Wei et al., 2012; Wang et al., 2013a; Wang et al., 2013b; Wang et al., 2014; Ren, 2013; Li et al., 2015; Zhang et al., 2016; Han et al., 2017; Wang et al., 2017; Yan and Lin, 2017; Bai et al., 2018; Yan et al., 2018; Sun et al., 2019) also supports GPS results, resulting in He et al. (2006) concluding that a uniform sinistral XFS had formed connected block boundaries. But the question of whether this uniform boundary has cut across the RRF is still in hot argument. It is widely accepted that the left-lateral strike-slip motion along the system is absorbed, or at least partially, by the deformation along the two parallel NW-trending faults, Qujiang fault and Shiping-Jianshui fault, before it reaches up to the RRF (He et al., 1993; Li, 1993; Wen et al., 2011; Wang et al., 2014) because of the unclear faulting geomorphological appearance of the XFS in the south area of Qujiang Fault. The XFS has been split into the east branch and the west branch in the south of Daduo (Shen et al., 2003). With the development of high-resolution satellite images and high-resolution topography reconstruction technology, our research team has revealed the strong Holocene faulting activity of the south segment of the XFS (Han et al., 2017; Guo et al., 2021a; Guo et al., 2021b), which could be treated as an elongation of the east branch of the XFS. Oppositely, the Holocene faulting research on the RRF (Li et al., 2016; Shi et al., 2018a) showed us very weak activity.

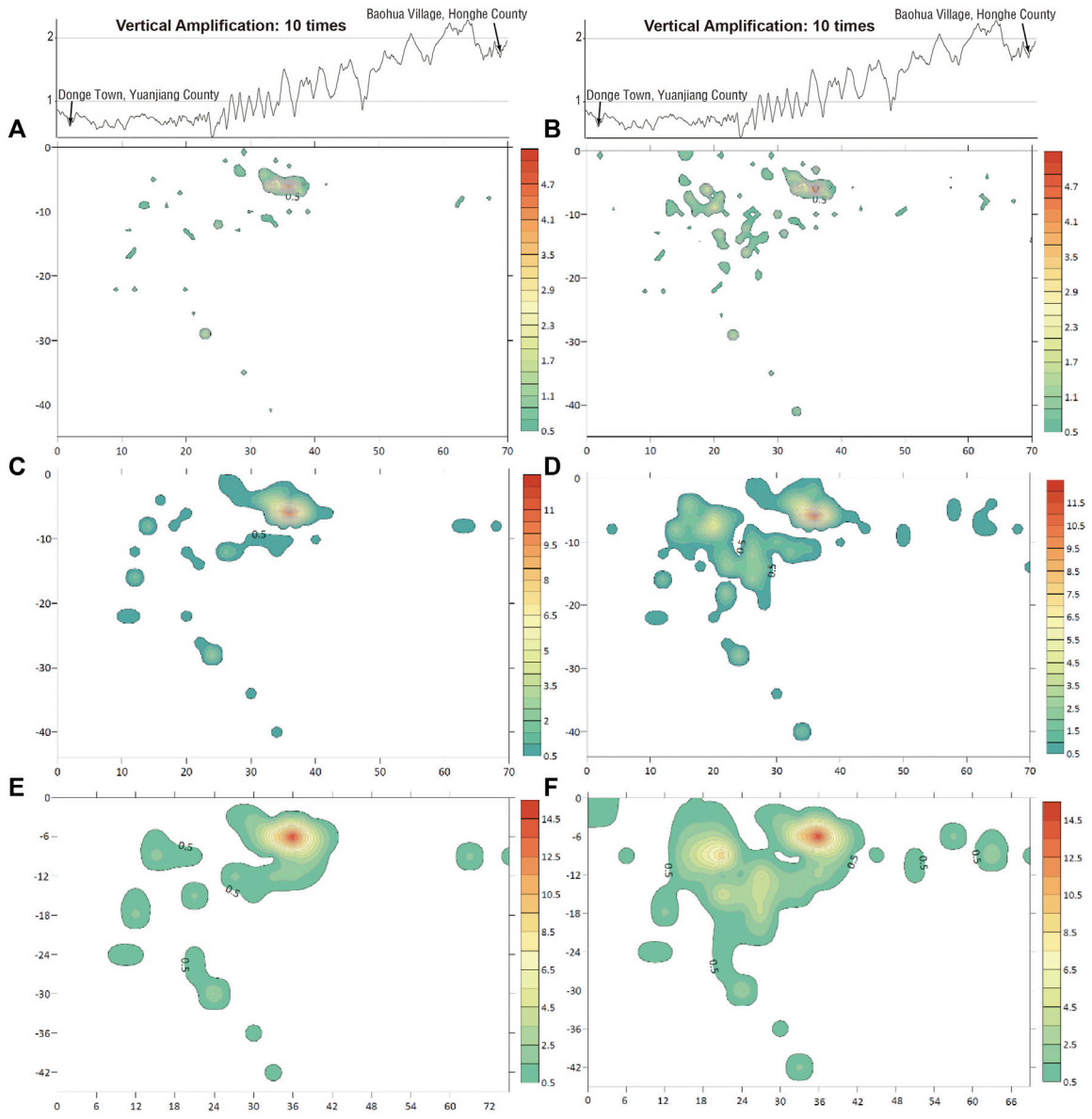

FIGURE 8
Earthquake energy isolines map along profile B-B′. The upper charts are the geomorphological profiles along B-B′ and their settlement sites. The left charts **(A,C,E)** are the results in the region on 10 km lateral sides of B-B′ while the right charts **(B,D,F)** are the results on 20 km. The mesh grid size of charts a and b is 1 km*1km, charts c and d is 2 km*2km, and charts e and f is 3 km*3 km. The unit of both axes is km.

Tectonic research on both fault systems in late Cenozoic Current research about initiation time of sinistral slip on XFS, such as paleomagnetic research in related basins (Yao et al., 2007; Zhu et al., 2008), and tectonic analysis (Wang et al., 1998), support the age as young as 4-5Ma. The tectonic inversion time of the RRF from left- to right-lateral motion (Lacassin et al., 1998; Fyhn and Phach, 2015; Wang et al., 2016) is believed to probably be 5-5.5Ma BP in Late Neogene, which is consistent with the sinistral initiation time of XFS. Isotope and fission-track studies (Roger et al., 1995; Zhang et al., 2004; Wang et al., 2009; Zhang et al., 2017) relating to shearing deformation in the Xianshuihe Fault area demonstrated two phases of thermo-emplacement events, 14-9Ma and 5Ma-present. All this evidence implies that the XFS propagated southwardly and started to tectonically affect the RRF at approximately 5Ma BP. A geological survey on NW-striking Qujiang Fault (Wang et al., 2014) demonstrated that it truncated the west branch of XFS and absorbed the shortening caused by the sinistral slip of the west branch of XFS.

The magnetotelluric imaging involving our study region (Bai et al., 2010) has revealed that two high conductivity channels exist in the southeast Tibetan Plateau, one of which developed along the west side of XFS and the south end of it has at least reached RRF. Shi et al. (2018b) summarized and analyzed all active faulting and GPS observations in the region's southwest side of the RRF and proposed the geodynamic model for that region, in which (Sippl et al., 2018) onal bookshelf faulting in the upper crust controlled by localized channel flow in deep crust was jointly driven by tongue-like asthenospheric flow with different

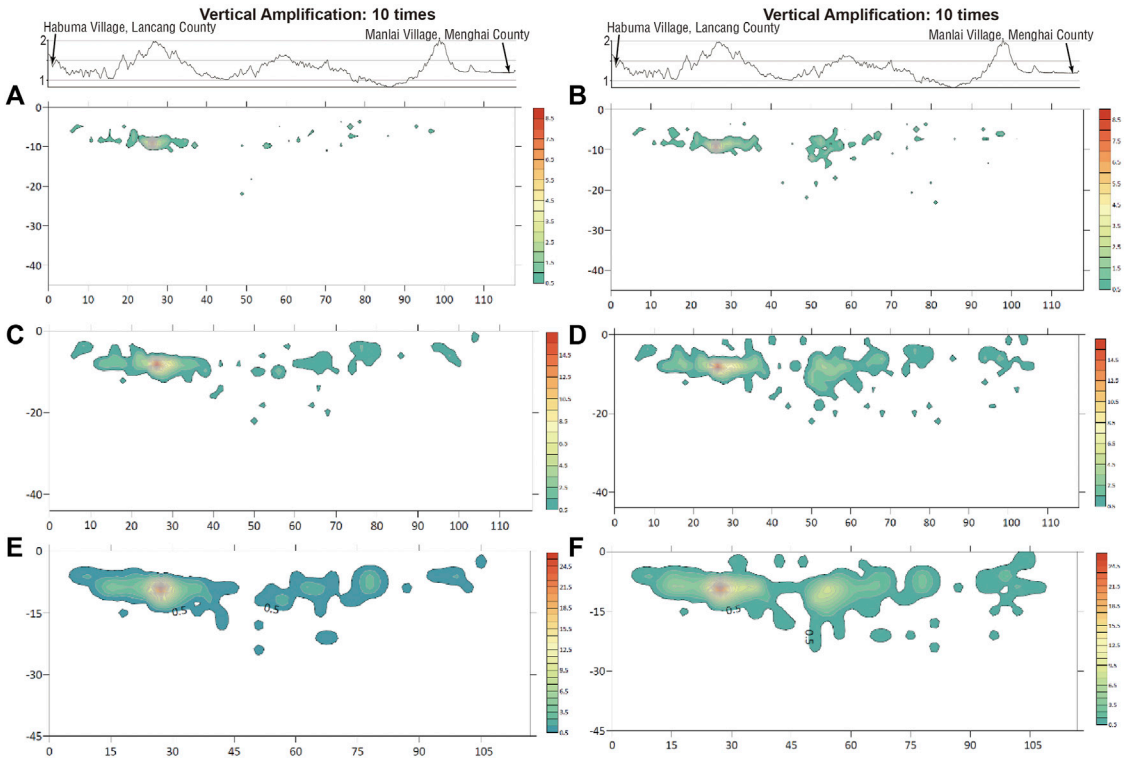

FIGURE 9
Earthquake energy isolines map along profile C-C′. The upper charts are the geomorphological profiles along C-C′ and their settlement sites. The left charts **(A,C,E)** are the results in the region in the 10 km lateral sides of C-C′ while the right charts **(B,D,F)** are the results on 20 km. The mesh grid size of charts a and b is 1 km*1km, charts c and d is 2 km*2 km, and charts e and f is 3 km*3 km. The unit of both axes is km.

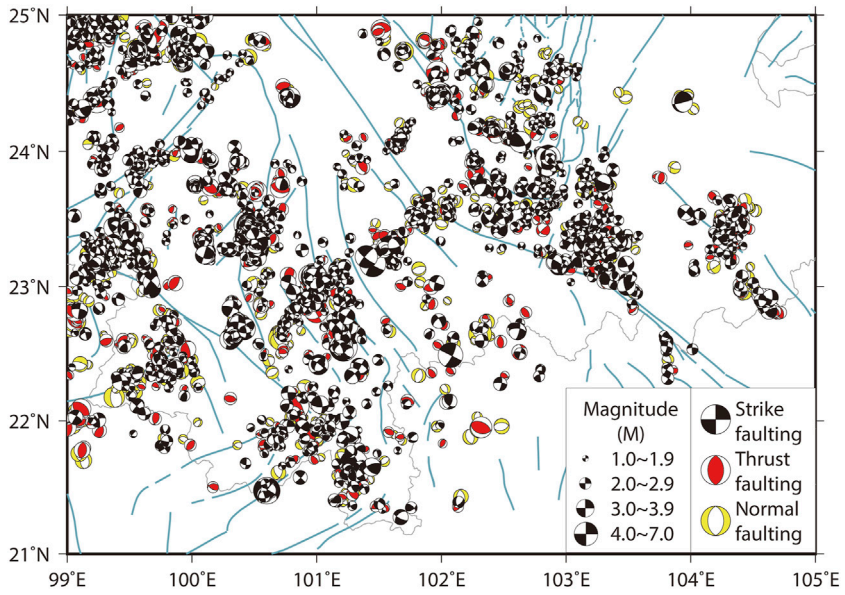

FIGURE 10
The focal mechanism solution results in the study region based on continuous waveform inversion.

TABLE 2 Classification table of focal mechanism solutions in the study region.

Dip-angle of the stress axis			Fault type	Number
P Axis	B Axis	T Axis		
Pl≥52°		Pl≤35°	Normal fault (NF)	1,089
40°≤Pl<52°		Pl≤20°	Normal fault with striking component (NS)	228
Pl<40°	Pl≥45°	Pl≤20°	Strike-slip Fault (SS)	1,368
Pl≤20°	Pl≥45°	Pl<40°	Strike-slip Fault (SS)	1,359
Pl≤20°		40°≤Pl≤52°	Thrust fault (TF)	209
Pl≤35°		Pl≥52°	Thrust with striking component (TS)	1,021

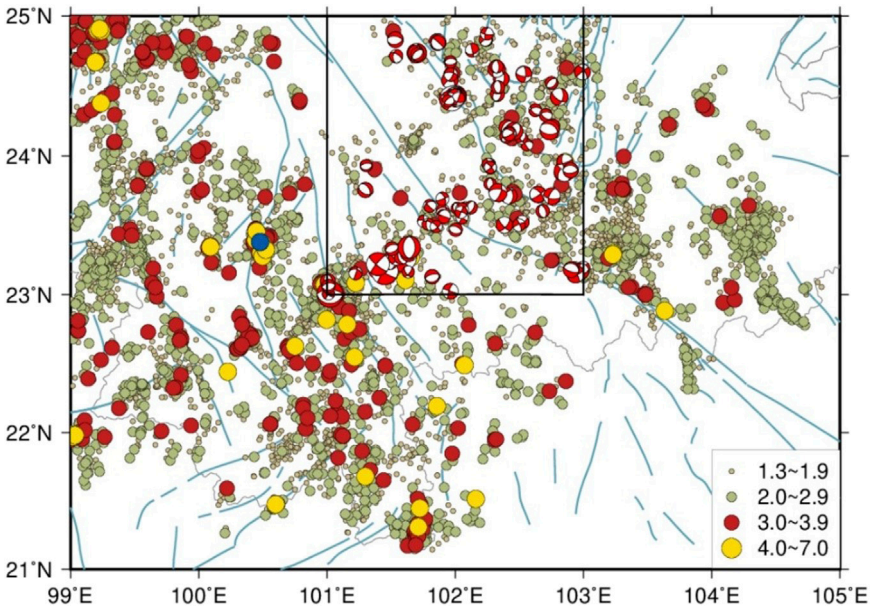

FIGURE 11
Focal mechanism solutions (ML≥2.0) distribution map in this study. The black rectangle is the study region of Hu and Han (2013).

flow velocities and SW-striking extrusion of Chuandian Block. The trace of the anomalous belt north of the RRF discovered in this study is consistent with the high conductivity revealed by Bai et al. (2010). The geodynamic model research on the north (Bai et al., 2010) and south (Shi et al., 2018b) of the RRF both emphasized the existence of deep channel flow. The shear wave splitting research on the Red River-Ailaoshan area (Huang et al., 2007) concluded that the upper mantle anisotropy to two sides of the Red River-Ailaoshan fault zone is different. Meanwhile, arrival data of the body waves research on the Red River-Ailaoshan area (Xu et al., 2005) showed that the metamorphic belt along the Red river-Ailaoshan fault zone appeared as high velocities from upper to middle crust, and deep dynamic conditions still placed constraints on the motion of the RRF. The receiver function analysis (Xu et al., 2006) on the Red River-Ailaoshan area verified that the RRF cut the whole crust and lower crust with low velocity existing there, meaning the possible existence of channel flow. At the same time, all GPS observation, especially the most updated observation (Figure 1; Gan et al., 2021), reflecting current earth surface deformation, seems to support the finding that the left-lateral shear of the region is not blocked, or at least is obviously absorbed by the and Gan et al. (2021) also proposed that convective removal of some or all of Tibet's mantle lithosphere probably was the main geodynamic driving force. So, combining all current geological and geophysical recognitions on this region and the geodynamic model proposed previously (Shi et al., 2018b), the following geodynamic model could be proposed here:

The asthenospheric flow is the basic driving force controlling the tectonic deformation in the crust. The comparatively weak channel flow along the west side of the XFS also affects the tectonic deformation in the upper crust of the Chuandian Block directly. Before 5-5.5Ma BP, sinistral slip movement of the XFS and RRF controlled the tectonic deformation in the Chuandian Block (Figure 16A). At approximately 5-

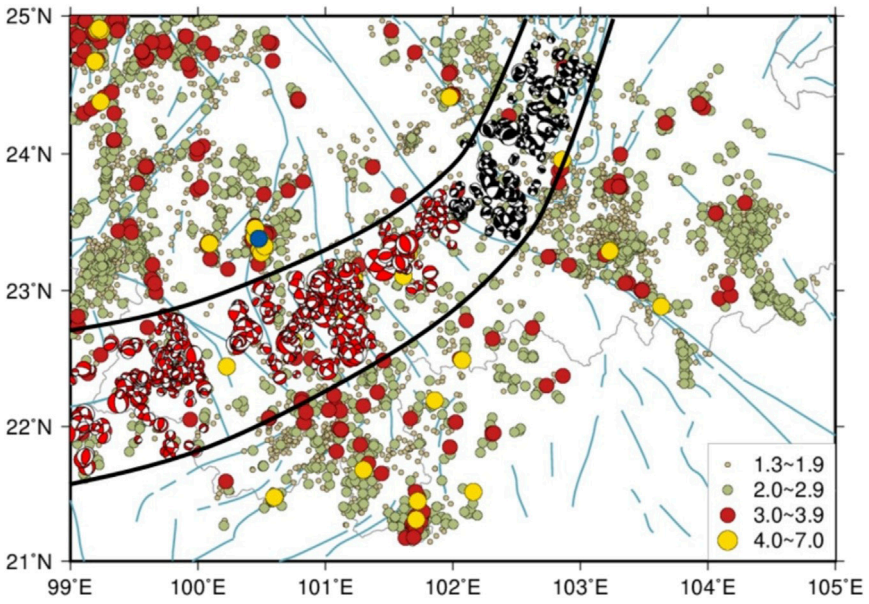

FIGURE 12
Focal mechanism solutions distribution map of subregions besides the RRF along the XFS and its elongation (ML≥1.3).

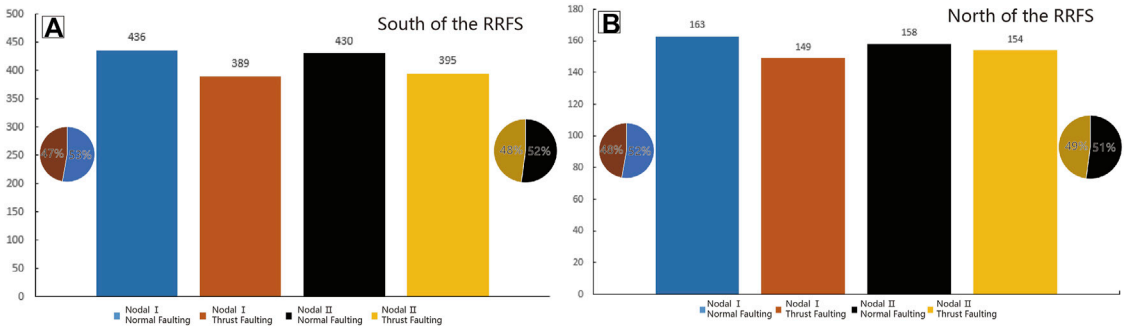

FIGURE 13
Statistical characteristics of two subregions besides the RRF, or south **(A)** and north **(B)** side.

5.5Ma BP, due to the joint effect of the extrusion from the EHS and the following asthenospheric flow adjustment, the sinistral slip movement of the XFS was enhanced, and the tectonic inversion from sinistral to dextral slip movement of RRF happened and started to propagate southwardly from the intersection between the east branch and Qujiang Fault (Figure 16B). The XFS in the upper crust probably reached the RRF recently, probably in Late Pleistocene (Guo et al., 2021b) and has been cutting through the RRF in the upper crust since then, which also can explain weak faulting geomorphological appearance of the south segment of the XFS (Figure 16C). In the southwest of the RRF, due to the geodynamic adjustment of this region, some regenerative faults are forming, such as the Longling-Lancang Fault (Guo et al., 1999). Figure 16.

The other interesting phenomenon revealed here is that the global velocity model (PREM model) fits better than the local model (HN model) (Table 1). Usually, the local velocity model is more suitable with the smallest error than the global model. But when the crust structure is too complicated and the local model cannot be representative, probably the global model is the better choice. The study area of the local HN model (23°-25°N, 101°20′-103°E) chosen in this study is much smaller than the study area in this study. The HN model only involved two first-order tectonic blocks, Chuandian Block and Indochina Block, while our study area involved three, Chuandian Block, Indochina Block, and South China Block (Figure 1A). This probably explains why the global model fits our study area better.

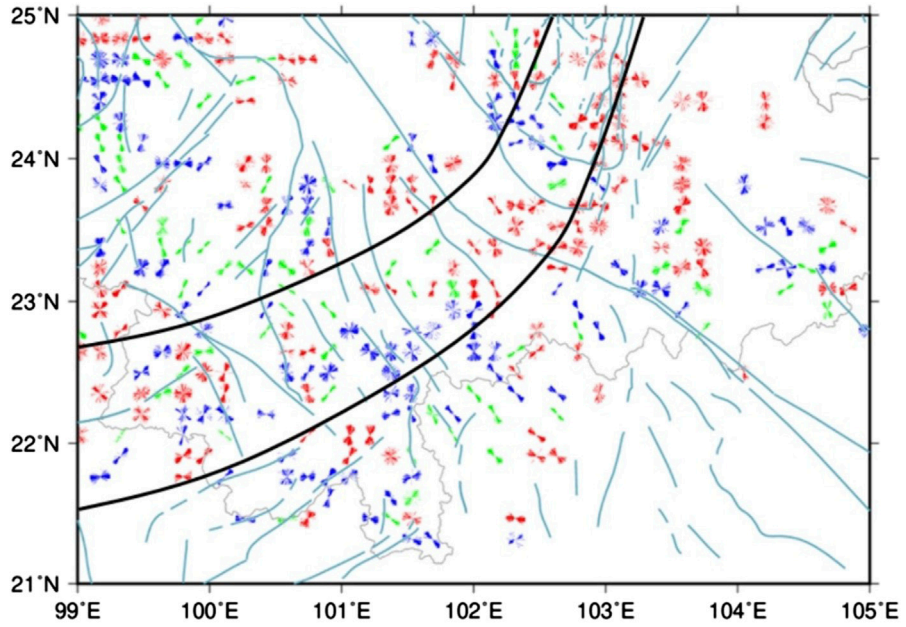

FIGURE 14
The direction distribution map of maximum horizontal principal compressive stress in the study region. Red is normal faulting, green is striking slip faulting, and blue is thrust faulting.

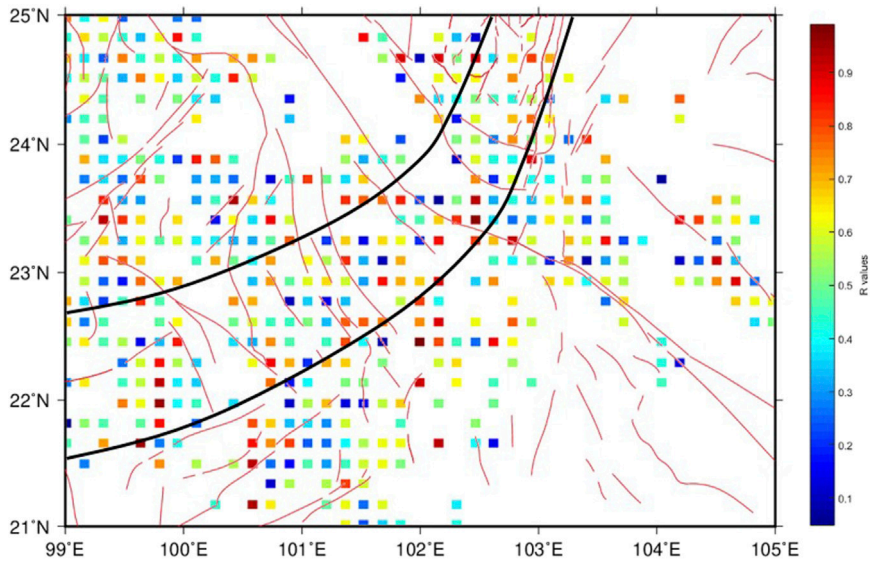

FIGURE 15
The R-value distribution map of the study region.

5 Conclusion

Based on seismic relocation, b-value analysis, seismic energy, density distribution research, focal mechanism solution inversion, and regional stress field study on the intersection area between the XFS and RRF, the following conclusion could be reached:

1) The XFS intersects with the RRF; earthquake activity and seismic energy are concentrated, and after crossing the RRF, the seismic density and energy distribution only slightly decreased. The statistical results of the focal mechanism solution are similar, both are predominate normal-striking-slip, and their stress field characteristics are consistent. It

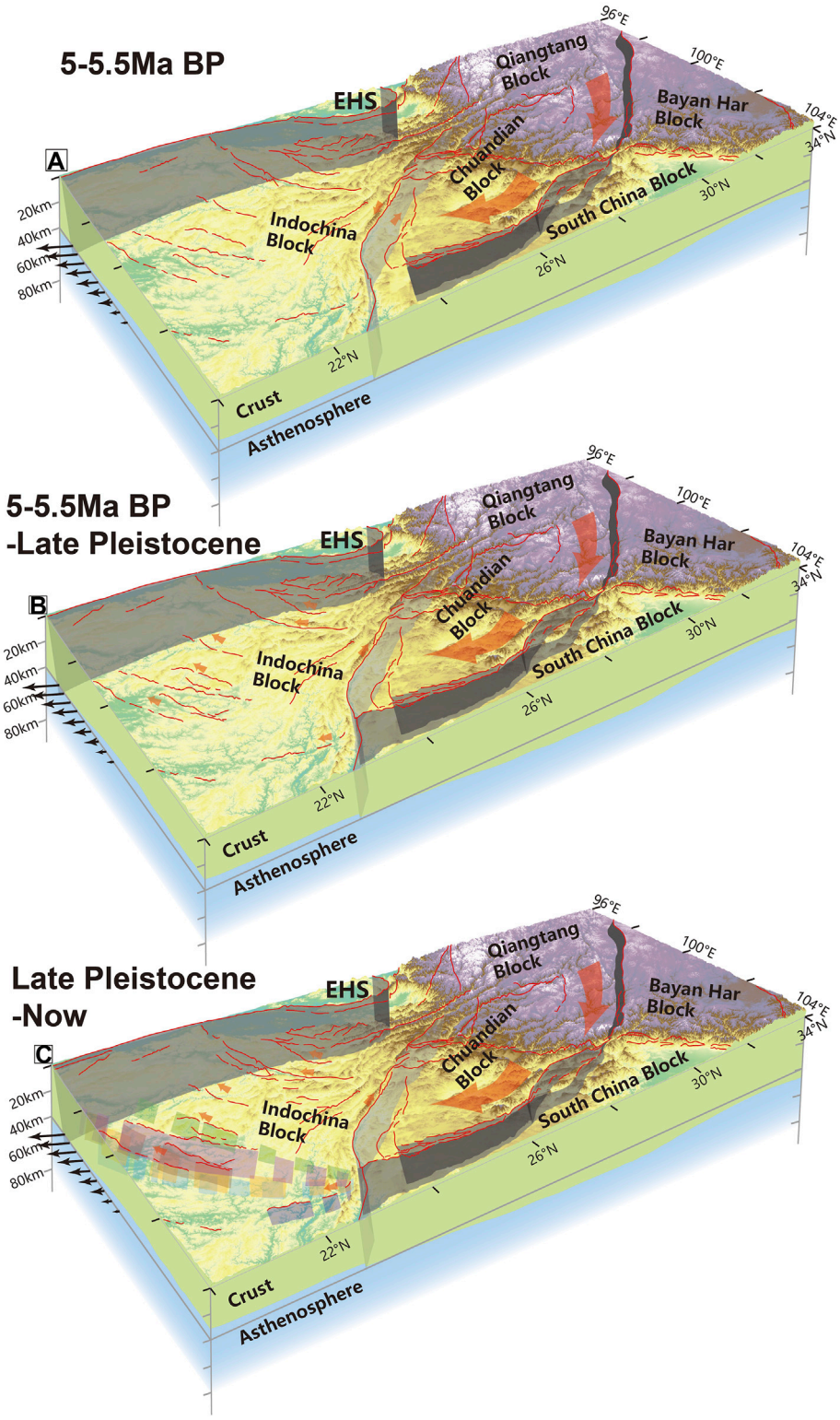

FIGURE 16
Proposed geodynamic evolution model from 5–5.5Ma BP **(A)**, 5–5.5Ma BP-Late Pleistocene **(B)** to Late Pleistocene- now **(C)**. The crust model is constructed based on previous geophysical results (Xu et al., 2005; Xu et al., 2006; Huang et al., 2007; Bai et al., 2010).

indicated that the southern section of the XFS has not been affected by the RRF, and it has continued for a length after crossing the RRF.

2) The seismic density distribution on both sides of the Dian Bien Phu fault zone is similar, the stress field features are consistent, and the sliding rate is small, while the seismic activity caused by

the fault extension after the XFS passes the RRF is quite different. Therefore, the Dian Bien Phu fault zone is not an extension fault of the XFS. The Dian Bien Phu fault zone and both sides of the zone should be included as a whole in the outer boundary block in the clockwise rotation dynamics model of the southeastern margin of the Tibetan Plateau.

3) Along the NE direction, starting from the middle segment of the XFS to the trans-Qujiang fault, Shiping-Jianshui fault zone, RRF, the Ailaoshan fault zone, the Wuliangshan fault zone, and the southern section of the Zhiyu-Puma fault zone, the seismic density and energy distribution are similar, and the R-value is stable. The profile density distribution shows that there is a structural belt with deep focal depth inside. This should be used as the eastern boundary of the clockwise rotational dynamics model of the Qinghai-Tibetan Plateau in this study area.
4) XFS is cutting across RRF nowadays, probably since the Late Pleistocene, which determines the key base of the geodynamic model in this region.

Data availability statement

The original contributions presented in the study are included in the article/Supplementary Material, further inquiries can be directed to the corresponding author.

Author contributions

SD did the fieldwork, processed the data, and wrote the manuscript. ZH and PG contributed to the conception and provided funding for the study. ZX helped draw the figures and analyze data. XY reviewed and edited the manuscript. All authors contributed to the article and approved the submitted version.

Funding

This research was supported by the National Natural Science Foundation of China (41772218) and the National Science and Technology Basic Resources Investigation Program of China (2021FY100103).

Acknowledgments

Our sincere thanks go to the editor and three reviewers, whose comments helped improve the manuscript a lot.

Conflict of interest

The authors declare that the research was conducted in the absence of any commercial or financial relationships that could be construed as a potential conflict of interest.

Publisher's note

Supplementary material

The Supplementary Material for this article can be found online at: https://www.frontiersin.org/articles/10.3389/feart.2023.1239689/full#supplementary-material

References

Bai, D., Unsworth, M. J., Meju, M. A., Ma, X., Teng, J., Kong, X., et al. (2010). Crustal deformation of the eastern Tibetan plateau revealed by magnetotelluric imaging. *Nat. Geosci.* 3, 358–362. doi:10.1038/ngeo830

Bai, M., Chevalier, M. L., Pan, J., Replumaz, A., Leloup, P. H., Métois, M., et al. (2018). Southeastward increase of the late Quaternary slip-rate of the Xianshuihe fault, eastern Tibet. Geodynamic and seismic hazard implications. *Earth Planet. Sci. Lett.* 485, 19–31. doi:10.1016/j.epsl.2017.12.045

Chen, Y., and Chen, H. (1999). "Fundamentals of seismic source theory, Class Lecture," in *School of earth and space sciences* (Beijing: Peking University).

Chen, Z., Burchfiel, B., Liu, Y., King, R., Royden, L., Tang, W., et al. (2000). Global Positioning System measurements from eastern Tibet and their implications for India/Eurasia intercontinental deformation. *J. Geophys. Res. Solid Earth* 105, 16215–16227. doi:10.1029/2000jb900092

Cheng, E. (1981). Recent tectonic stress field and tectonic movement of the Sichuan Province and its vicinity (in Chinese with English abstract). *Acta Seismol. Sin.* 3 (3), 231–241.

Cheng, W., Diao, G., Lu, Y., Zhang, Y., Li, G., and & Chen, T. (2003). Focal mechanisms, displacement rate and mode of motion of the Sichuan-Yunnan block (in Chinese with English abstract). *Seismol. Geol.* 25 (1), 71–87. doi:10.3969/j.issn.0253-4967.2003.01.008

Copley, A. (2008). Kinematics and dynamics of the southeastern margin of the Tibetan Plateau. *Geophys. J. Int.* 174, 1081–1100. doi:10.1111/j.1365-246x.2008.03853.x

Dziewonski, A. M., and Anderson, D. L. (1981). Preliminary reference Earth model. *Phys. earth Planet. interiors* 25, 297–356. doi:10.1016/0031-9201(81)90046-7

Flesch, L. M., Haines, A. J., and Holt, W. E. (2001). Dynamics of the India-Eurasia collision zone. *J. Geophys. Res. Solid Earth* 106, 16435–16460. doi:10.1029/2001jb000208

Fyhn, M. B., and Phach, P. V. (2015). Late Neogene structural inversion around the northern gulf of tonkin, vietnam: effects from right-lateral displacement across the Red River fault zone. *Tectonics* 34, 290–312. doi:10.1002/2014tc003674

Gan, W., Molnar, P., Zhang, P., Xiao, G., Liang, S., Zhang, K., et al. (2021). Initiation of clockwise rotation and eastward transport of southeastern Tibet inferred from deflected fault traces and GPS observations. *GSA Bull.* 134, 1129–1142. doi:10.1130/b36069.1

Guo, P., Han, Z., Dong, S., Gao, F., and Li, J. (2021a). New constraints on slip behavior of the Jianshui strike-slip fault from faulted stream channel risers and airborne lidar data, SE Tibetan plateau, China. *Remote Sens.* 13, 2019. doi:10.3390/rs13102019

Guo, P., Han, Z., Dong, S., Mao, Z., Hu, N., Gao, F., et al. (2021b). Latest quaternary active faulting and paleoearthquakes on the southern segment of the Xiaojiang Fault Zone, SE Tibetan plateau. *Lithosphere* 2021, 6379. doi:10.2113/2021/7866379

Guo, S., Zhou, R., and Xiang, H. (1999). Longling-lancang fault zone in southwest yunnan: A new rupture zone on the continental crust (in Chinese). *Chin. Sci. Bull.* 44 (19), 2118–2121.

Guo, X., Chen, X., Wang, S., and Wang, H. (2014). Waffle-cone technique using solitaire AB stent for endovascular treatment of complex and wide-necked bifurcation cerebral aneurysms. *China Earthq. Eng. J.* 36 (3), 599–602. doi:10.1111/jon.12121

Gutenberg, B., and Richter, C. F. (1944). Frequency of earthquakes in California. *Bull. Seismol. Soc. Am.* 34, 185–188. doi:10.1785/bssa0340040185

Han, Z., Dong, S., Mao, Z., Hu, N., Tan, X., Yuan, R., et al. (2017). The Holocene activity and strike-slip rate of the southern segment of Xiaojiang Fault in the southeastern Yunnan region, China (in Chinese with English abstract). *Seismol. Geol.* 39 (1), 1–16. doi:10.3969/j.issn.0253-4967.2017.01.001

Hardebeck, J. L., and Michael, A. J. (2004). Stress orientations at intermediate angles to the san andreas fault, California. *J. Geophys. Res. Solid Earth* 109, 3239. doi:10.1029/2004jb003239

He, H. L., and Ikeda, Y. (2007). Faulting on the Anninghe fault zone, southwest China in late quaternary and its movement model. *Acta Seismol. Sin.* 20, 571–583. doi:10.1007/s11589-007-0571-4

He, H., Fang, Z., and Li, P. (1993). A preliminary approach to the fault activity of southern segment on Xiaojiang west branch Fault (in Chinese with English abstract). *J. Seismol. Res.* 16 (3), 291–298.

He, H., Ikeda, Y., He, Y., Togo, M., Chen, J., Chen, C., et al. (2008). Newly-generated daliangshan fault zone—shortcutting on the central section of Xianshuihe-Xiaojiang fault system. *Sci. China Ser. D Earth Sci.* 51, 1248–1258. doi:10.1007/s11430-008-0094-4

He, H., Li, P., and Fang, Z. (1992). Analysis of seismogenic conditions in the wedge tectonic region of southeast Yunnan Province (in Chinese with English abstract). *Seismol. Geol.* 14 (3), 217–226.

He, H., and Oguchi, T. (2008). Late Quaternary activity of the Zemuhe and Xiaojiang faults in southwest China from geomorphological mapping. *Geomorphology* 96, 62–85. doi:10.1016/j.geomorph.2007.07.009

He, H., Ran, H., and Ikeda, Y. (2006). Uniform strike-slip rate along the Xianshuihe-Xiaojiang Fault System and its implications for active tectonics in southeastern Tibet. *Acta Geol. Sin. Engl. Ed.* 80, 376–386. doi:10.1111/j.1755-6724.2006.tb00255.x

He, H., and Ren, J. (2003). Holocene earthquakes on the Zemuhe Fault in southwestern China. *Ann. Geophys.* 46, 1035–1052. doi:10.4401/ag-3444

Hu, N., and Han, Z. (2013). Seismological study on behaviors of present-day movement of arcuate tectonic belt in southeast Yunnan (in Chinese with English abstract). *Seismology and Geology* 35 (1), 1–21.

Huang, J., Wan, Y., Sheng, S., Li, X., and &Gao, X. (2016). Heterogeneity of present-day stress field in the Tonga-Kermadec subduction zone and its geodynamic significance (in Chinese with English abstract). *Chin. J. Geophys.* 59 (2), 578–592.

Huang, Z., Wang, L., Xu, M., Liu, J., Mi, N., and Liu, S. (2007). Shear wave splitting across the Ailao Shan-Red River fault zone, SW China. *Geophys. Res. Lett.* 34, L20301. doi:10.1029/2007gl031236

Iwakuni, M., Kato, T., Takiguchi, H., Nakaegawa, T., and Satomura, M. (2004). Crustal deformation in Thailand and tectonics of Indochina peninsula as seen from GPS observations. *Geophys. Res. Lett.* 31, 347. doi:10.1029/2004gl020347

Kan, R., Zhang, S., Yan, F., and Yu, L. (1977). Present tectonic stress field and its relation to the characteristics of recent tectonic activity in southwestern China (in Chinese with English abstract). *Chin. J. Geophys.* 20 (2), 96–109.

Kennett, B. L., Engdahl, E., and Buland, R. (1995). Constraints on seismic velocities in the Earth from traveltimes. *Geophys. J. Int.* 122, 108–124. doi:10.1111/j.1365-246x.1995.tb03540.x

Lacassin, R., Replumaz, A., and Leloup, P. H. (1998). Hairpin river loops and slip-sense inversion on southeast Asian strike-slip faults. *Geology* 26, 703–706. doi:10.1130/0091-7613(1998)026<0703:hrlass>2.3.co;2

Li, P. (1993). *The Xianshuihe-Xiaojiang Fault Zone*. Beijing: Seismological Press.

Li, P., and Wang, L. (1975). Exploration of the seismo-geological features of the Yunnan-west Sichuan region (in Chinese with English abstract). *Chin. J. Geol.* 1975 (04), 308–326.

Li, X., Ran, Y., Chen, L., Wang, H., Yu, J., Zhang, Y., et al. (2016). The Holocene seismic evidence on southern segment of the red river fault zone (in Chinese with English abstract). *Seismol. Geol.* 38 (3), 596–604. doi:10.3969/j.issn.0253-4967.2016.03.007

Li, X., Ran, Y., Chen, L., Wu, F., Ma, X., and Cao, J. (2015). Late quaternary large earthquakes on the western branch of the Xiaojiang Fault and their tectonic implications. *Acta Geol. Sin. Engl. Ed.* 89, 1516–1530. doi:10.1111/1755-6724.12561

Lund, B., and Townend, J. (2007). Calculating horizontal stress orientations with full or partial knowledge of the tectonic stress tensor. *Geophys. J. Int.* 170, 1328–1335. doi:10.1111/j.1365-246x.2007.03468.x

Luo, J., Zhao, C., and Zhou, L. (2014). Characteristics of focal mechanisms and stress field of the Chuan-Dian rhombic block and its adjacent regions (in Chinese with English abstract). *Seismol. Geol.* 36 (2), 17. doi:10.3969/j.issn.0253-4967.2014.02.011

Molnar, P., and Tapponnier, P. (1975). Cenozoic Tectonics of Asia: effects of a Continental Collision: features of recent continental tectonics in Asia can be interpreted as results of the India-Eurasia collision. *Science* 189, 419–426. doi:10.1126/science.189.4201.419

Paige, C. C., and Saunders, M. A. (1982). Lsqr: an algorithm for sparse linear equations and sparse least squares. *ACM Trans. Math. Softw. (TOMS)* 8, 43–71. doi:10.1145/355984.355989

Peltzer, G., and Tapponnier, P. (1988). Formation and evolution of strike-slip faults, rifts, and basins during the India-asia collision: an experimental approach. *J. Geophys. Res. Solid Earth* 93, 15085–15117. doi:10.1029/jb093ib12p15085

Ren, Z. (2013). Geometry and deformation features of the most recent co-seismic surface ruptures along the Xiaojiang Fault and its tectonic implications for the Tibetan Plateau. *J. Asian Earth Sci.* 77, 21–30. doi:10.1016/j.jseaes.2013.08.016

Ren, Z., Lin, A., and Rao, G. (2010). Late pleistocene–holocene activity of the Zemuhe Fault on the southeastern margin of the Tibetan plateau. *Tectonophysics* 495, 324–336. doi:10.1016/j.tecto.2010.09.039

Replumaz, A., Lacassin, R., Tapponnier, P., and Leloup, P. (2001). Large river offsets and Plio-Quaternary dextral slip rate on the Red River fault (Yunnan, China). *J. Geophys. Res.* 106, 819–836. doi:10.1029/2000jb900135

Replumaz, A., and Tapponnier, P. (2003). Reconstruction of the deformed collision zone between India and Asia by backward motion of lithospheric blocks. *J. Geophys. Res. Solid Earth* 108, 1978–2012. doi:10.1029/2001jb000661

Roger, F., Calassou, S., Lancelot, J., Malavieille, J., Mattauer, M., Zhiqin, X., et al. (1995). Miocene emplacement and deformation of the konga Shan granite (xianshui He fault zone, west sichuan, China): geodynamic implications. *Earth Planet. Sci. Lett.* 130, 201–216. doi:10.1016/0012-821x(94)00252-t

Royden, L. H., Burchfiel, B. C., King, R. W., Wang, E., Chen, Z., Shen, F., et al. (1997). Surface deformation and lower crustal flow in eastern Tibet. *science* 276, 788–790. doi:10.1126/science.276.5313.788

Rydelek, P. A., and Sacks, I. S. (1989). Testing the completeness of earthquake catalogues and the hypothesis of self-similarity. *Nature* 337, 251–253. doi:10.1038/337251a0

Schoenbohm, L. M., Burchfiel, B. C., and Liangzhong, C. (2006). Propagation of surface uplift, lower crustal flow, and Cenozoic tectonics of the southeast margin of the Tibetan Plateau. *Geology* 34, 813–816. doi:10.1130/g22679.1

Schoenbohm, L., Whipple, K., Burchfiel, B., and Chen, L. (2004). Geomorphic constraints on surface uplift, exhumation, and plateau growth in the Red River region, Yunnan Province, China. *Geol. Soc. Am. Bull.* 116, 895–909. doi:10.1130/b25364.1

Seismic ground motion parameter zonation map of China (2015). *National standard, state administration for market regulation*. Beijing, China: Standards Press of China.

Shao, Y., Yuan, D., and Liang, M. (2015). Seismic risk assessment of the Longling-Lancang fault zone, southwestern Yunnan (in Chinese with English abstract). *Acta Seismol. Sin.* 37 (6), 1011–1023. doi:10.11939/jass.2015.06.011

Shen, J., Wang, Y., and Song, F. (2003). Characteristics of the active Xiaojiang fault zone in yunnan, China: A slip boundary for the southeastward escaping sichuan–yunnan block of the Tibetan plateau. *J. Asian Earth Sci.* 21, 1085–1096. doi:10.1016/s1367-9120(02)00185-2

Shen, Z. K., Lü, J., Wang, M., and Bürgmann, R. (2005). Contemporary crustal deformation around the southeast borderland of the Tibetan Plateau. *J. Geophys. Res. Solid Earth* 110, 1978–2012. doi:10.1029/2004jb003421

Shi, X., Sieh, K., Weldon, R., Zhu, C., Han, Y., Yang, J., et al. (2018a). Slip rate and rare large prehistoric earthquakes of the Red River Fault, southwestern China. *Geochem. Geophys. Geosystems* 19, 2014–2031. doi:10.1029/2017gc007420

Shi, X., Wang, Y., Sieh, K., Weldon, R., Feng, L., Chan, C. H., et al. (2018b). Fault slip and GPS velocities across the Shan Plateau define a curved southwestward crustal motion around the eastern Himalayan syntaxis. *J. Geophys. Res. Solid Earth* 123, 2502–2518. doi:10.1002/2017jb015206

Simons, W., Socquet, A., Vigny, C., Ambrosius, B., Haji Abu, S., Promthong, C., et al. (2007). A decade of GPS in southeast asia: resolving sundaland motion and boundaries. *J. Geophys. Res. Solid Earth* 112, B06420. doi:10.1029/2005jb003868

Sippl, C., Schurr, B., Asch, G., and Kummerow, J. (2018). Seismicity structure of the northern Chile forearc from> 100,000 double-difference relocated hypocenters. *J. Geophys. Res. Solid Earth* 123, 4063–4087. doi:10.1002/2017jb015384

Song, F., and Wang, Y. (1998). *The active Xiaojiang fault zone*. Seismological Press. Beijing: Seismological Press.

Sun, H., He, H., Ikeda, Y., Wei, Z., Chen, C., Xu, Y., et al. (2019). Paleoearthquake history along the southern segment of the daliangshan Fault Zone in the southeastern Tibetan plateau. *Tectonics* 38, 2208–2231. doi:10.1029/2018tc005009

Tapponnier, P., Peltzer, G., Dain, A. Y. L., Armijo, R., and Cobbold, P. (1982). Propagating extrusion tectonics in Asia:New insights from simple experiments with plasticine. *Geology* 10, 611–616. doi:10.1130/0091-7613(1982)10<611:petian>2.0.co;2

Waldhauser, F., and Ellsworth, W. L. (2000). A double-difference earthquake location algorithm: method and application to the northern hayward fault, California. *Bull. Seismol. Soc. Am.* 90, 1353–1368. doi:10.1785/0120000006

Wang, D., Wu, S., Li, C., and Yao, G. (2016). Submarine slide evidence for late Miocene strike-slip reversal of the Red River Fault. *Sci. China Earth Sci.* 59, 2231–2239. Boulder, CO: Geological Society of America. doi:10.1007/s11430-015-5534-9

Wang, E., Burchfiel, B. C., Royden, L. H., Chen, L., Chen, J., Li, W., et al. (1998). *Late cenozoic xianshuihe-xiaojiang, Red River, and dali fault systems of southwestern sichuan and central yunnan, China*. Boulder, CO: Geological Society of America.

Wang, H., Ran, Y., Chen, L., and Li, Y. (2017). Paleoearthquakes on the Anninghe and Zemuhe fault along the southeastern margin of the Tibetan Plateau and implications for

fault rupture behavior at fault bends on strike-slip faults. *Tectonophysics* 721, 167–178. doi:10.1016/j.tecto.2017.08.030

Wang, H., Ran, Y., Li, Y., and Chen, L. (2013a). Paleoseismic ruptures and evolution of a small triangular pull-apart basin on the Zemuhe fault. *Sci. China Earth Sci.* 56, 504–512. doi:10.1007/s11430-012-4543-8

Wang, H., Ran, Y., Li, Y., Gomez, F., and Chen, L. (2014a). A 3400-year-long paleoseismologic record of earthquakes on the southern segment of Anninghe fault on the southeastern margin of the Tibetan plateau. *Tectonophysics* 628, 206–217. doi:10.1016/j.tecto.2014.04.040

Wang, H., Ran, Y., Li, Y., Gomez, F., and Chen, L. (2013b). Holocene palaeoseismologic record of earthquakes on the Zemuhe fault on the southeastern margin of the Tibetan Plateau. *Geophys. J. Int.* 193, 11–28. doi:10.1093/gji/ggs095

Wang, S., Fang, X., Zheng, D., and Wang, E. (2009). Initiation of slip along the Xianshuihe fault zone, eastern Tibet, constrained by K/Ar and fission-track ages. *Int. Geol. Rev.* 51, 1121–1131. doi:10.1080/00206810902945132

Wang, Y., Wang, E., Shen, Z., Wang, M., Gan, W., Qiao, X., et al. (2008). GPS-constrained inversion of present-day slip rates along major faults of the Sichuan-Yunnan region, China. *Sci. China Ser. D Earth Sci.* 51, 1267–1283. doi:10.1007/s11430-008-0106-4

Wang, Y., Zhang, B., Hou, J., and Xu, X. (2014b). Structure and tectonic geomorphology of the Qujiang fault at the intersection of the Ailao Shan–Red River fault and the Xianshuihe–Xiaojiang fault system, China. *Tectonophysics* 634, 156–170. doi:10.1016/j.tecto.2014.07.031

Wei, Z., He, H., Shi, F., Xu, Y., Bi, L., and Sun, H. (2012). Cardamonin protects septic mice from acute lung injury by preventing endothelial barrier dysfunction. *Seismol. Geol.* 34 (2), 282–290. doi:10.1002/jbt.21420

Wen, X., Du, F., Long, F., Fan, J., and Zhu, H. (2011). Tectonic dynamics and correlation of major earthquake sequences of the Xiaojiang and Qujiang-Shiping fault systems, Yunnan, China (in Chinese). Sci. China Ser. D *Earth Sci.* 41 (5), 713–724. doi:10.1007/s11430-011-4231-0

Wu, Z., Long, C., Fan, T., Zhou, C., Feng, H., Yang, Z., et al. (2015). The arc rotational-shear active tectonic system on the southeastern margin of Tibetan Plateau and its dynamic characteristics and mechanism (in Chinese with English abstract). *Geol. Bull. China* 34 (01), 1–31. doi:10.3969/j.issn.1671-2552.2015.01.002

Xie, F., Cui, X., Zhao, J., Chen, Q., and Li, H. (2004). Regional division of the recent tectonic stress field in China and adjacent areas (in Chinese with English abstract). *Chin. J. Geophys.* 47 (4), 654–662. doi:10.3321/j.issn:0001-5733.2004.04.016

Xu, J. (1995). Earthquake mechanisms and its implication for tectonic stress field in the southern part of the North-South seismic belt in China (in Chinese). *Acta Seismol. Sin.* 17 (1), 31–40.

Xu, M., Wang, L., Liu, J., Zhong, K., Li, H., Hu, D., et al. (2006). Crust and uppermost mantle structure of the Ailaoshan-Red River fault from receiver function analysis. *Sci. China Ser. D Earth Sci.* 49, 1043–1052. doi:10.1007/s11430-006-1043-8

Xu, X., Wen, X., Zheng, R., Ma, W., Song, F., and Yu, G. (2003). Pattern of latest tectonic motion and its dynamics for active blocks in Sichuan-Yunnan region, China (in Chinese). *Sci. China(Series D)* 33 (01), 151–162. doi:10.3321/j.issn:1006-9267.2003.z1.017

Xu, Y., Liu, J., Liu, F., Song, H., Hao, T., and Jiang, W. (2005). Crust and upper mantle structure of the Ailao Shan-Red River fault zone and adjacent regions. *Sci. China Ser. D Earth Sci.* 48, 156–164. doi:10.1360/02yd0386

Xu, Z., Wang, S., Huang, Y., and Gao, A. (1989). The tectonic stress field of Chinese continent deduced from a great number of earthquakes (in Chinese with English abstract). *Chin. J. Geophys.* 32 (6), 636–647.

Xu, Z., Yang, J., Li, H., Ji, S., Zhang, Z., and Liu, Y. (2011). On the tectonics of the India-asia collision (in Chinese with English abstract). *Acta Geol. Sin.* 85 (1), 1–33.

Yan, B., Jia, D., and Lin, A. (2018). Late pleistocene-holocene tectonic landforms developed along the strike-slip Xianshuihe Fault Zone, Tibetan plateau, China. *J. Geodyn.* 120, 11–22. doi:10.1016/j.jog.2018.05.005

Yan, B., and Lin, A. (2017). Holocene activity and paleoseismicity of the selaha fault, southeastern segment of the strike-slip Xianshuihe Fault Zone, Tibetan plateau. *Tectonophysics* 694, 302–318. doi:10.1016/j.tecto.2016.11.014

Yao, H., Zhao, Z., Qiao, Y., Li, C., Wang, S., Wang, Y., et al. (2007). Magnetostraphic dating of the xigeda formation in mianning, sichuan and its significance. *Quat. Sci.* 27, 74–84.

Yao, Z. S., Roberts, R. G., and Tryggvason, A. (1999). Calculating resolution and covariance matrices for seismic tomography with the LSQR method. *Geophys. J. Int.* 138, 886–894. doi:10.1046/j.1365-246x.1999.00925.x

Yin, A., and Harrison, T. M. (2000). Geologic evolution of the Himalayan-Tibetan orogen. *Annu. Rev. Earth Planet. Sci.* 28, 211–280. doi:10.1146/annurev.earth.28.1.211

Zhang, J., and Ding, Z. (2016). Discussion about several issues on dien bien Phu Fault & north-south seismic belt (in Chinese with English abstract). *J. Seismol. Res.* 39 (4), 527–536.

Zhang, P. Z., Shen, Z., Wang, M., Gan, W., Bürgmann, R., Molnar, P., et al. (2004a). Continuous deformation of the Tibetan Plateau from global positioning system data. *Geology* 32, 809–812. doi:10.1130/g20554.1

Zhang, P., Deng, Q., Zhang, G., Ma, J., Gan, W., Min, W., et al. (2003). Active tectonic blocks and strong earthquakes in the continent of China (in Chinese). Sci. China Ser. D *Earth Sci.* 46 (2), 13–24. doi:10.1360/03dz0002

Zhang, Y. Z., Replumaz, A., Leloup, P. H., Wang, G. C., Bernet, M., Van Der Beek, P., et al. (2017). Cooling history of the gongga batholith: implications for the Xianshuihe Fault and miocene kinematics of SE Tibet. *Earth Planet. Sci. Lett.* 465, 1–15. doi:10.1016/j.epsl.2017.02.025

Zhang, Y., Chen, W., and Yang, N. (2004b). $^{40}Ar/^{39}Ar$ dating of shear deformation of the Xianshuihe fault zone in west Sichuan and its tectonic significance (in Chinese). *Sci. China Ser. D Earth Sci.* 34 (7), 613–632. doi:10.1109/tmi.2004.826359

Zhang, Y., Yao, X., Yu, K., Du, G., and Guo, C. (2016). Late-quaternary slip rate and seismic activity of the Xianshuihe Fault Zone in southwest China. *Acta Geol. Sin. - Engl. Ed.* 90, 525–536. doi:10.1111/1755-6724.12688

Zheng, Y., and Yang, J. (2008). Analysis of double-difference algorithm and the effect of its parameter in location (in Chinese with English abstract). *Seismol. Geomagnetic Observation Res.* 29 (3), 85–93. doi:10.3969/j.issn.1003-3246.2008.03.016

Zhu, R., Potts, R., Pan, Y., Lü, L., Yao, H., Deng, C., et al. (2008). Paleomagnetism of the Yuanmou Basin near the southeastern margin of the Tibetan Plateau and its constraints on late Neogene sedimentation and tectonic rotation. *Earth Planet. Sci. Lett.* 272, 97–104. doi:10.1016/j.epsl.2008.04.016

Zoback, M. L. (1992). First-and second-order patterns of stress in the lithosphere: the world stress map project. *J. Geophys. Res. Solid Earth* 97, 11703–11728. doi:10.1029/92jb00132